Article

#-CuVO Nanowires: Hydrothermal Synthesis and Primary Lithium Battery Application

Hua Ma, Shaoyan Zhang, Weiqiang Ji, Zhanliang Tao, and Jun Chen

J. Am. Chem. Soc., **2008**, 130 (15), 5361-5367 • DOI: 10.1021/ja800109u • Publication Date (Web): 26 March 2008

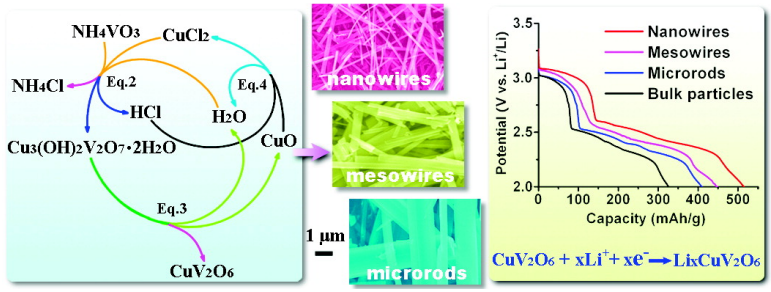

More About This Article

Additional resources and features associated with this article are available within the HTML version:

- Supporting Information
- Links to the 2 articles that cite this article, as of the time of this article download
- Access to high resolution figures
- Links to articles and content related to this article
- Copyright permission to reproduce figures and/or text from this article

View the Full Text HTML

J|A|C|S
ARTICLES

Published on Web 03/26/2008

α-CuV_2O_6 Nanowires: Hydrothermal Synthesis and Primary Lithium Battery Application

Hua Ma, Shaoyan Zhang, Weiqiang Ji, Zhanliang Tao, and Jun Chen*

Key Laboratory of Energy-Material Chemistry (Tianjin) and Engineering Research Center of Energy Storage & Conversion (Ministry of Education), Chemistry College, Nankai University, Tianjin 300071, People's Republic of China

Received January 6, 2008; E-mail: chenabc@nankai.edu.cn

Abstract: We report on the synthesis, characterization, and electrochemical lithium intercalation of α-CuV_2O_6 nanowires, mesowires, and microrods that were prepared through a facile hydrothermal route. The diameters of the as-synthesized α-CuV_2O_6 nanowires, mesowires, and microrods were about 100 nm, 400 nm, and 1 μm, respectively. It was found that by simply controlling the hydrothermal reaction parameters, such as the reagent concentration and the dwell time, the transformation of microrods to nanowires was readily achieved via a "ripening−splitting" mechanism. Electrochemical measurements revealed that the as-prepared α-CuV_2O_6 nanowires and mesowires displayed high discharge capacities (447−514 mAh/g at 20 mA/g and 37 °C) and excellent high-rate capability. In particular, the α-CuV_2O_6 nanowires showed capacities much higher than those of α-CuV_2O_6 mesowires, microrods, and bulk particles. The mechanisms for the electrochemical lithium intercalation into the α-CuV_2O_6 nanowires were also discussed. From the Arrhenius plot of lithium intercalation into α-CuV_2O_6 nanowires, the activation energies were calculated to be 39.3 kJ/mol at 2.8 V (low lithium uptake) and 35.7 kJ/mol at 2.3 V (high lithium uptake). This result indicates that the α-CuV_2O_6 nanowires are promising cathode candidates for primary lithium batteries used in long-term implantable cardioverter defibrillators (ICD).

Introduction

The primary and secondary batteries, which are electrically connected electrochemical cells having terminals/contacts to supply electrical energy, have gained tremendous importance for powering the society today.[1,2] For example, an implantable cardioverter defibrillator (ICD), which is a special device that monitors the heart rhythms of patients and delivers shocks if dangerous rhythms are detected, needs the batteries to provide power sources (see Supporting Information Figure S1). Since the ICD is widely used nowadays to effectively protect patients against cardiovascular disease, which caused at least 16.7 million or 29.2% of total global deaths every year according to World Health Report 2003,[3] the batteries play important roles in prolonging the life of the patients. Among various batteries, the Li/$Ag_2V_4O_{11}$ primary batteries are dominating the ICD today owing to their high energy density, high power, and long-term stability. However, the batteries used in ICD still meet more stringent requirements including larger discharge capacity, higher power capability, and longer lifespans,[4] with responses to this challenge lying mainly in advanced materials.[5] Indeed, recent studies on $Ag_4V_2O_6F_2$,[6] hybrid $Ag_2V_4O_{11}$−CF_x,[7] and $Ag_2V_4O_{11}$ nanowires[8] have displayed enhanced electrochemical activity including the improvement on the discharge capacity and high-rate capability. This result means that seeking $Ag_2V_4O_{11}$ alternative materials with high capacity is of great scientific and technological importance.

Among the potential candidates, copper vanadate (CuV_2O_6) has the layered structure and multistep reductions during the insertion/intercalation of lithium, which are similar to the character of $Ag_2V_4O_{11}$. In addition, the presence of two-electron transfer during the reduction from Cu^{2+} to Cu^0 and the lighter molecular weight of CuV_2O_6 offer the possibility of higher gravimetric capacity and energy density than that of $Ag_2V_4O_{11}$.[9] The discharge capacity of the irregular CuV_2O_6 microparticles prepared by solid-state reaction or solution-based route is hardly up to 350 mAh/g to the cutoff voltage of 2.0 V.[10] The limitations to the discharge capacity of CuV_2O_6 microparticles are primarily due to the sluggish kinetics of lithium intercalation (diffusion) into the electrode during the discharge process.

(1) (a) Bard, A. J.; Faulkner, L. R. *Electrochemical Methods Fundamentals and Applications*; John Wiley & Sons: 2003. (b) Linden, D.; Reddy, T. B. *Handbook of Batteries*; McGraw-Hill: New York, 2002.
(2) (a) Ogasawara, T.; Débart, A.; Holzapfel, M.; Novák, P.; Bruce, P. G. *J. Am. Chem. Soc.* **2006**, *128*, 1390. (b) Winter, M.; Brodd, R. J. *Chem. Rev.* **2004**, *104*, 4245. (c) Ferrigno, R.; Stroock, A. D.; Clark, T. D.; Mayer, M.; Whitesides, G. M. *J. Am. Chem. Soc.* **2002**, *124*, 12930. (d) Tarascon, J. M.; Armand, M. *Nature* **2001**, *414*, 359.
(3) The World Health Report 2003 from World Health Organization (WHO) on the website, http://www.who.int/whr/2003/en/Chapter6-en.pdf.
(4) Crespi, A.; Schmidt, C.; Norton, J.; Chen, K. M.; Skarstad, P. *J. Electrochem. Soc.* **2001**, *148*, A30.
(5) Long, J. W.; Dunn, B.; Rolison, D. R.; White, H. S. *Chem. Rev.* **2004**, *104*, 4463.
(6) Sorensen, E. M.; Izumi, H. K.; Vaughey, J. T.; Stern, C. L.; Poeppelmeier, K. R. *J. Am. Chem. Soc.* **2005**, *127*, 6347.
(7) Chen, K. M.; Merritt, D. R.; Howard, W. G.; Schmidt, C. L.; Skarstad, P. M. *J. Power Sources* **2006**, *162*, 837.
(8) Zhang, S. Y.; Li, W. Y.; Li, C. S.; Chen, J. *J. Phys. Chem. B* **2006**, *110*, 24855.
(9) Morcrette, M.; Rozier, P.; Dupont, L.; Mugnier, E.; Sannier, L.; Galy, J.; Tarascon, J. M. *Nat. Mater.* **2003**, *2*, 755.

Since the hydrothermal synthesis is an effective method for the chemical synthesis of nanostructured materials with well-controlled shapes, sizes, and structures[11] and, furthermore, since nanostructured materials have been encouraged for possible use in energy storage and conversion,[12,13] here we report on the systematic studies of the hydrothermal synthesis of shape/size-controlled α-CuV_2O_6 nanowires, mesowires, and microrods and the electrochemical performance of Li/CuV_2O_6 primary batteries. The results show that the as-synthesized α-CuV_2O_6 nanowires exhibited high discharge capacity, superior high-rate capability, and enhanced kinetics toward lithium intercalation, making them one of the most promising cathode candidates for lithium primary batteries in the application of implantable cardioverter defibrillators (ICD).

Experimental Section

Synthesis and Characterization. The α-CuV_2O_6 nanowires were synthesized through a hydrothermal route from the reaction of $CuCl_2$ and NH_4VO_3 in a Teflon-lined autoclave (Supporting Information Figure S2). The overall chemical reaction involved in the hydrothermal synthesis can be briefly described in eq 1.

$$CuCl_2 + 2NH_4VO_3 \rightarrow \alpha\text{-}CuV_2O_6 + 2NH_4Cl \quad (1)$$

All of the chemical reagents were of analytical grade and used without further purification. In a typical preparation of α-CuV_2O_6 nanowires, 0.48 mmol $CuCl_2 \cdot 2H_2O$ was dissolved into 8 mL of deionized water at room temperature, while 0.96 mmol NH_4VO_3 was dissolved into another 8 mL of deionized water at 80 °C. Then, the NH_4VO_3 solution (0.12 mol/L) was added slowly to the $CuCl_2$ solution (0.06 mol/L) under stirring. A yellow precipitate formed immediately. After continuous stirring for 10 min, the resulting precursor suspension was transferred into a 25 mL Teflon-lined autoclave and maintained at 210 °C for 12 h. After being cooled to ambient temperature naturally, the solid powder in the autoclave was collected by centrifugation, washed several times with deionized water and ethanol, and finally vacuum-dried at 60 °C for 4 h. The parameters of the hydrothermal reaction, such as the concentration of the reactants and the reaction time, were also investigated in order to understand the growth mechanism of the α-CuV_2O_6 nanowires. Table 1 summarizes the experimental conditions and the corresponding morphology and phase of the products. For comparison, α-CuV_2O_6 bulk particles were prepared by mixing V_2O_5 and CuO powders in a molar ratio of 1:1 and then calcined at 620 °C in air for 48 h, according to the solid-state reaction reported previously.[14]

Table 1. Summary of the Experimental Conditions and the Corresponding Morphology and Phase of the Products

time (h)	concentration of $CuCl_2$ (mol/L)[a]	morphology	phase
0	0.06	nanoparticles	$Cu_3(OH)_2V_2O_7 \cdot 2H_2O$
1	0.06	nanoparticles and lamellar structure	$Cu_3(OH)_2V_2O_7 \cdot 2H_2O$
3	0.06	splitted nanosheets	CuV_2O_6 and $Cu_3(OH)_2V_2O_7 \cdot 2H_2O$
6	0.06	splitted nanowires	CuV_2O_6 and $Cu_3(OH)_2V_2O_7 \cdot 2H_2O$
12	0.06	nanowires	CuV_2O_6
12	0.03	nanowires	CuV_2O_6
12	0.1	nanowires	CuV_2O_6
12	0.15	mesowires	CuV_2O_6
12	0.01	microrods	CuV_2O_6

[a] The concentration ratio of $CuCl_2$ and NH_4VO_3 solution was maintained at 1:2 in all of the experimental conditions.

The phase of the as-prepared samples was investigated by powder X-ray diffraction (XRD, Rigaku D/max-2500 X-ray generator, Cu Kα radiation). The XRD profiles were refined by the Rietveld refinement program RIETAN-2000.[15] The morphology and microstructure of the as-synthesized samples were analyzed with scanning electron microscopy (SEM, JEOL JSM-6700F Field Emission, 10 kV), transmission electron microscopy (TEM), and high-resolution TEM (Philips Tecnai FEI 20, 200 kV). The specific surface areas of the products were detected by Brunauer–Emmett–Teller (BET) nitrogen adsorption–desorption measurements (Shimadzu-Micrometrics ASAP 2010). The oxidation states of the constituent elements were measured with X-ray photoelectron spectroscopy (XPS) using Mg Kα radiation at an accelerating voltage of 13 kV and a pass energy of 35.75 eV (PHI, PHI5300 system), in which the XPSPEAK software was used for the fitting of the XPS spectra.

Electrochemical Measurements. The working electrode was fabricated by mixing the active materials (namely, the as-prepared α-CuV_2O_6 nanowires, mesowires, microrods, or bulk particles), carbon black (Cabort, Vulcon XC-72), and ploytetrafluoroethylene (PTFE) in the weight ratio of 85:10:5. Then, the mixture was coated onto a nickel foam. After solvent evaporation at room temperature and drying in a vacuum oven at 110 °C for 24 h, the electrodes were assembled into coin-like cells (CR2032) with lithium metal as the counter and reference electrode. The electrolyte solution was 1.0 mol/L $LiPF_6$ dissolved in a mixture of ethylene carbonate (EC) and diethyl carbonate (DEC) solution with the volumetric ratio of EC/DEC = 1:1. The cells were constructed and handled in an Ar (99.999%)-filled glovebox (Mikrouna Co., Ltd., Universal).

The capacity of the electrode was measured by a galvanostatic discharge method at different current densities to the cutoff voltage of 2.0 V, which was performed through an Arbin charge–discharge unit at the temperature of 37 °C. The capacity was based on the amount of the active material, excluding the weight of the additives in the electrode. The cyclic voltammogram (CV) was performed on a Parstat 2273 potentiostat/galvanostat analyzer (Princeton Applied Research & AMTECT Company) at a scanning rate of 1 mV/s and the temperature of 37 °C. The electrochemical impedance spectroscopy (EIS) was also investigated by the Parstat 2273 potentiostat/galvanostat analyzer with an AC voltage of 10 mV amplitude in the frequency range from 1×10^5 to 1×10^{-2} Hz.[16] Prior to EIS measurement, the as-assembled cells were discharged to the requested voltage (2.8 or 2.3 V vs Li^+/Li) and held for 4 h to reach the equilibrium state at 25, 37, 45, or 55 °C. The EIS data were analyzed using ZsimpWin software. The cells at the discharged

(10) (a) Takeda, Y.; Itoh, K.; Kanno, R.; Icikawa, T.; Imanishi, N.; Yamamoto, O. *J. Electrochem. Soc.* **1991**, *138*, 2566. (b) Andrukaitis, E.; Cooper, J. P.; Smit, J. H. *J. Power Sources* **1995**, *54*, 465. (c) Wei, Y. J.; Ryu, C. W.; Chen, G.; Kim, K. B. *Electrochem. Solid-States Lett.* **2006**, *9*, A487. (d) Cao, X. Y.; Xie, J. G.; Zhan, H.; Zhou, Y. H. *Mater. Chem. Phys.* **2006**, *98*, 71.

(11) (a) Parnham, E. R.; Morris, R. E. *Acc. Chem. Res.* **2007**, *40*, 1005. (b) Song, H.; Rioux, R. M.; Hoefelmeyer, J. D.; Komor, R.; Niesz, K.; Grass, M.; Yang, P. D.; Somorjai, G. A. *J. Am. Chem. Soc.* **2006**, *128*, 3027. (c) Wang, X.; Zhuang, J.; Peng, Q.; Li, Y. D. *Nature* **2005**, *437*, 121. (d) Gur, I.; Fromer, N. A.; Geier, M. L.; Alivisatos, A. P. *Science* **2005**, *310*, 462. (e) Duxin, N.; Liu, F. T.; Vali, H.; Eisenberg, A. *J. Am. Chem. Soc.* **2005**, *127*, 10063. (f) Cushing, B. L.; Kolesnichenko, V. L.; O'Connor, C. J. *Chem. Rev.* **2004**, *104*, 3893. (g) Feng, S. H.; Xu, R. R. *Acc. Chem. Res.* **2001**, *34*, 239.

(12) (a) Li, J.; Tang, S. B.; Lu, L.; Zeng, H. C. *J. Am. Chem. Soc.* **2007**, *129*, 9401. (b) Ma, H.; Cheng, F. Y.; Chen, J.; Zhao, J. Z.; Li, C. S.; Tao, Z. L.; Liang, J. *Adv. Mater.* **2007**, *19*, 4067. (c) Sides, C. R.; Martin, C. R. *Adv. Mater.* **2005**, *17*, 125. (d) Aricò, A. S.; Bruce, P.; Scrosati, B.; Tarascon, J. M.; Schalkwijk, W. V. *Nat. Mater.* **2005**, *4*, 366. (e) Bréger, J.; Dupré, N.; Chupas, P. J.; Lee, P. L.; Proffen, T.; Parise, J. B.; Grey, C. P. *J. Am. Chem. Soc.* **2005**, *127*, 7529.

(13) (a) Tenne, R. *Nat. Nanotechnol.* **2006**, *1*, 103. (b) Forster, P. M.; Eckert, J.; Heiken, B. D.; Parise, J. B.; Yoon, J. W.; Jhung, S. H.; Chang, J. S.; Cheetham, A. K. *J. Am. Chem. Soc.* **2006**, *128*, 16846. (c) Hu, X.; Skadtchenko, B. O.; Trudeau, M.; Antonelli, D. M. *J. Am. Chem. Soc.* **2006**, *128*, 11740.

(14) Sakurai, Y.; Ohtsuka, H.; Yamaki, J. I. *J. Electrochem. Soc.* **1988**, *135*, 32.

(15) Izumi, F.; Ikeda, T. *Mater. Sci. Forum* **2000**, *321–324*, 198.

(16) Li, W. Y.; Li, C. S.; Zhou, C. Y.; Ma, H.; Chen, J. *Angew. Chem., Int. Ed.* **2006**, *45*, 6009.

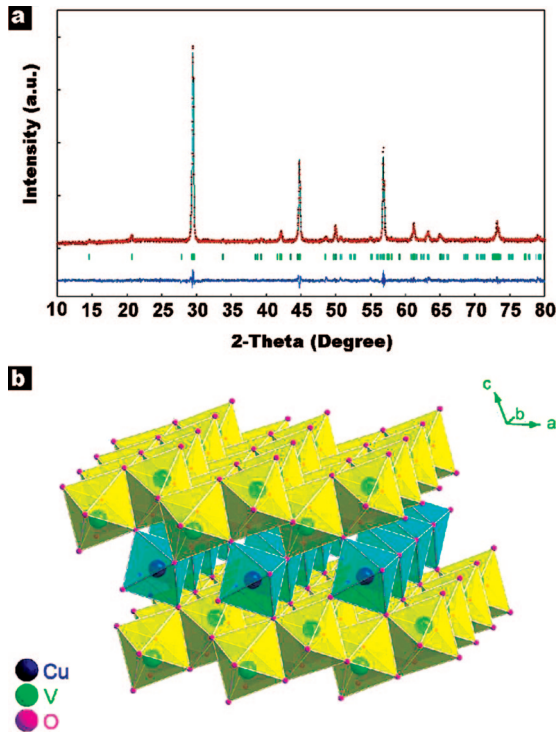

Figure 1. Structure analyses of α-CuV_2O_6 nanowires: (a) Rietveld refinement of XRD profiles with observed intensity (red line), calculated intensity (blue line), the positions of all possible reflection peaks (vertical bars in the middle), and the difference between the calculated and observed intensities (the bottom blue line). (b) Crystal structure with the vanadium−oxygen octahedra (yellow) and the copper−oxygen octahedra (light blue).

state were opened in an Ar-filled glovebox, and the materials scratched off the electrodes were analyzed by XPS and XRD with the prevention of oxygen and moisture.[17]

Results and Discussion

Structure and Morphology. Figure 1a shows the Rietveld refinement of the XRD pattern for the as-prepared α-CuV_2O_6 nanowires. All the diffraction peaks in the experimental pattern can be indexed to a triclinic phase of α-CuV_2O_6. No peaks from other phases have been detected, indicating the high purity of the product. The Rietveld refinement of the XRD pattern fits the experimental data points very well (Rwp = 8.79, S = 1.2157). The cell parameters of α-CuV_2O_6 can be determined to be a = 9.171(3) Å, b = 3.546(2) Å, c = 6.482(5) Å, α = 92.32(1)°, β = 110.32(4)°, and γ = 91.84(7)°, which are in good agreement with the standard values [space group: $P\bar{1}$ (No. 2), JCPDS-ICDD Card No. 30-0513]. The crystal structure of α-CuV_2O_6(Figure 1b) consists of VO_6 octahedral double layers along the b-direction. The Cu cations lie in the interlayer space, coordinating with six oxygen atoms to build CuO_6 octahedral chains, which are separated from each other by VO_6 octahedral double chains.

Panels a and b of Figure 2 show the typical SEM images of the as-synthesized α-CuV_2O_6 nanowires obtained at 210 °C for 12 h. The overview image (Figure 2a) shows that the nanowires have a uniform diameter along their entire length, which can be up to tens of micrometers. Moreover, these nanowires are interconnected to form a porous network architecture. The

(17) (a) Li, W. Y.; Xu, L. N.; Chen, J. *Adv. Funct. Mater.* **2006**, *15*, 851. (b) Chen, J.; Kurimara, N.; Xu, Q.; Takeshita, H. T.; Sakai, T. *J. Phys. Chem. B* **2001**, *105*, 11214.

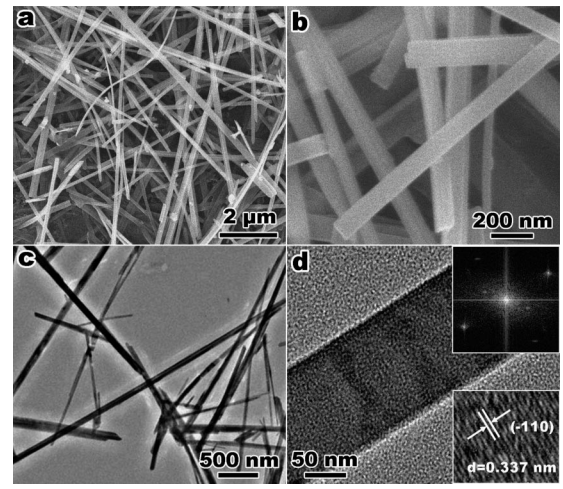

Figure 2. (a, b) SEM, (c) TEM, and (d) HRTEM images of the as-synthesized α-CuV_2O_6 nanowires. The bottom inset in (d) shows the lattice fringes, and the top inset shows the corresponding FFT pattern.

magnified SEM image in Figure 2b further confirms the uniformity of the α-CuV_2O_6 nanowires, with an average diameter of about 100 nm. Some of the nanowires are bundled. The morphology and microstructure of the α-CuV_2O_6 nanowires were further analyzed by TEM and HRTEM. The TEM image in Figure 2c shows that the diameters of the nanowires are around 100 nm, which are consistent with the observation in SEM images. From the HRTEM image of an individual nanowire in Figure 2d, the clear lattice fringes perpendicular to the longitudinal direction of the nanowire with an interplanar distance of 0.337 nm can be seen (the bottom inset of Figure 2d), which is in accordance with the d-spacing of the (-110) crystal planes. This result is further confirmed in the corresponding fast Fourier transform (FFT) pattern (the top inset of Figure 2d).

Furthermore, the diameter of the as-synthesized CuV_2O_6 one-dimensional (1-D) nanostructures can be controlled by altering the initial concentration of the reactants. It was found that the CuV_2O_6 nanowires with a diameter of about 100 nm were always obtained by maintaining the concentration of $CuCl_2$ solution in the range of 0.03–0.10 mol/L (Figure 2 and Supporting Information Figure S3). When the concentration of $CuCl_2$ solution was increased to 0.15 mol/L, the CuV_2O_6 mesowires with a diameter of approximately 400–500 nm were created (Supporting Information Figure S4a,b). In comparison, when the concentration of $CuCl_2$ solution was decreased to 0.01 mol/L, CuV_2O_6 microrods with a diameter of about 1 μm were formed (Supporting Information Figure S4c,d). To compare the electrochemical properties, bulk α-CuV_2O_6 with average particle sizes of about 10 μm were synthesized from solid-state reaction (Supporting Information Figure S5). The specific surface areas of α-CuV_2O_6 nanowires, mesowires, microrods, and bulk particles were measured to be 62.1, 12.6, 4.0, and 1.6 m^2/g, respectively.

Formation Mechanism. Up to now, since 1-D CuV_2O_6 nanostructures have rarely been investigated, the formation mechanism of α-CuV_2O_6 nanowires would be of particular interest. In the present synthesis, neither templates nor surfactants were used in the reaction system. To study the formation mechanism of α-CuV_2O_6 nanowires, time-dependent evolutions of crystal structure and morphology at 210 °C were studied by XRD and SEM (Supporting Information Figures S6 and S7).

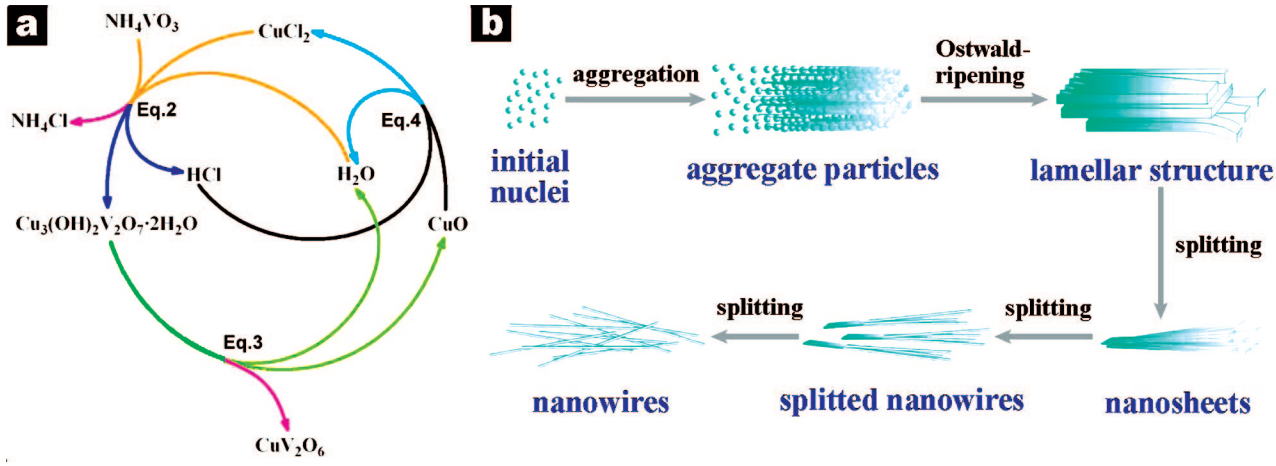

Figure 3. Schematic illustration of the (a) chemical reactions and (b) growth mechanism in the synthesis of α-CuV_2O_6 nanowires.

On the basis of the experimental results, the overall chemical reaction (eq 1) for the synthesis of α-CuV_2O_6 nanowires was proposed to divide into three steps, as formulated in eqs 2−4, respectively. The whole reaction process is described in Figure 3a. Initially, $Cu_3(OH)_2V_2O_7{\cdot}2H_2O$ nuclei are spontaneously formed through the reaction of $CuCl_2$ and NH_4VO_3 (eq 2). Next, $Cu_3(OH)_2V_2O_7{\cdot}2H_2O$ gradually decomposes into CuV_2O_6, CuO, and H_2O (eq 3) under the hydrothermal condition. Meanwhile, the resultant CuO (from eq 3) and HCl (from eq 2) convert to $CuCl_2$ (eq 4), which react with the residual NH_4VO_3 to make the "reaction circle" progress until NH_4VO_3 is consumed completely.

Thus, an Ostwald ripening and splitting process was proposed to elucidate the growth mechanism of the α-CuV_2O_6 nanowires (Figure 3b). In the initial stage, $Cu_3(OH)_2V_2O_7{\cdot}2H_2O$ nuclei are produced, aggregated, and grown into lamellar microstructures, as indicated by the sample at early stages (Supporting Information Figure S7a−d). This process is in accordance with the well-known "Ostwald ripening mechanism".[18] With the reaction processing, "a splitting process" occurs, in which the layered $Cu_3(OH)_2V_2O_7{\cdot}2H_2O$ gradually split into CuV_2O_6 nanosheets and splitted nanowires (Supporting Information Figure S7e−h), accompanied by a phase transformation from $Cu_3(OH)_2V_2O_7{\cdot}2H_2O$ to CuV_2O_6 (Supporting Information Figure S8). This process is driven by the H_2O molecular deintercalating from the interlayer spaces of $Cu_3(OH)_2V_2O_7{\cdot}2H_2O$. Finally, the α-$CuV_2O_6$ nanowires with uniform diameters are formed. Such a similar "ripening−splitting" process has occurred for the creation of $AgVO_3$, V_2O_5, and TiO_2 1-D nanostructures.[8,19,20]

$$3CuCl_2 + 2NH_4VO_3 + 5H_2O \rightarrow Cu_3(OH)_2V_2O_7 \cdot 2H_2O + 2NH_4Cl + 4HCl \quad (2)$$

$$Cu_3(OH)_2V_2O_7 \cdot 2H_2O \rightarrow CuV_2O_6 + 2CuO + 3H_2O \quad (3)$$

$$CuO + 2HCl \rightarrow CuCl_2 + H_2O \quad (4)$$

Electrochemical Properties. It is widely accepted that the electrochemcial properties of the electrode materials depend intimately on their morphologies and sizes.[21] Figure 4 shows the initial discharge curves of the electrodes with α-CuV_2O_6 nanowires, mesowires, microrods, and bulk particles at the current density of 20 mA/g and the temperature of 37 °C. The four electrodes exhibit a similar profile for the discharge curves with two voltage plateaus and two sloping voltage ranges. However, the open circuit voltages of α-CuV_2O_6 nanowires and mesowires are about 3.10 V, which are nearly 100 mV higher than that of α-CuV_2O_6 microrods and bulk particles. To the cutoff voltage of 2.0 V, the discharge capacities of the α-CuV_2O_6 electrodes are in the order of nanowires > mesowires > microrods > bulk particles (Table 2). The initial discharge capacity of α-CuV_2O_6 nanowires was 514 mAh/g, which is equivalent to an intercalation of approximately 5.0 Li per formula unit (~$Li_{5.0}CuV_2O_6$) according to the Faraday equation. In comparison, the discharge capacities of α-CuV_2O_6 mesowires and microrods were 447 and 409 mAh/g, respectively, which are still much higher than that for either the as-synthesized bulk particles (326 mAh/g) or the previously reported bulk CuV_2O_6[10d] and $Ag_2V_4O_{11}$.[22] From Table 2, one can also see that, at higher current densities of 40 and 80 mA/g (Supporting Information

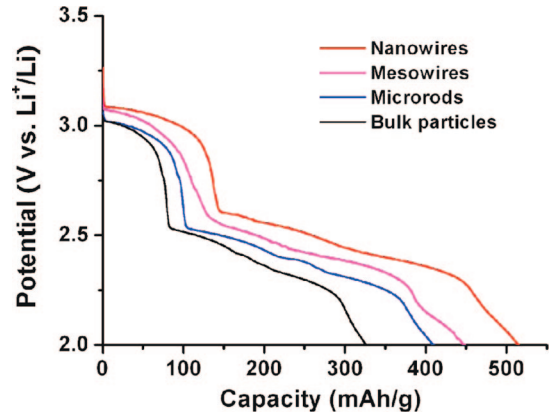

Figure 4. Discharge curves of the cells made from the as-prepared α-CuV_2O_6 nanowires, mesowires, microrods, and bulk particles at the current density of 20 mA/g and the temperature of 37 °C.

(18) (a) Li, J.; Zeng, H. C. *J. Am. Chem. Soc.* **2007**, *129*, 15839. (b) Li, R. F.; Luo, Z. T.; Papadimitrakopoulos, F. *J. Am. Chem. Soc.* **2006**, *128*, 6280. (c) Peng, Z. A.; Peng, X. G. *J. Am. Chem. Soc.* **2001**, *123*, 1389. (d) Narayanan, R.; El-Sayed, M. A. *J. Am. Chem. Soc.* **2003**, *125*, 8340.

(19) Li, B. X.; Xu, Y.; Rong, G. X.; Jing, M.; Xie, Y. *Nanotechnology* **2006**, *17*, 2560.

(20) Wu, D.; Liu, J.; Zhao, X. N.; Li, A. D.; Chen, Y. F.; Ming, N. B. *Chem. Mater.* **2006**, *18*, 547.

(21) Taberna, P. L.; Mitra, S.; Poizot, P.; Simon, P.; Tarascon, J. M. *Nat. Mater.* **2006**, *5*, 567. (b) Nam, K. T.; Kim, D. W.; Yoo, P. J.; Chiang, C. Y.; Meethong, N.; Hammond, P. T.; Chiang, Y. M.; Belcher, A. M. *Science* **2006**, *312*, 885. (c) Martin, C. R. *Science* **1994**, *266*, 1961.

Table 2. Comparison of Electrochemical Properties between the As-Synthesized α-CuV_2O_6 Samples (Nanowires, Mesowires, Microrods, and Bulk Particles) and the Previously Reported CuV_2O_6 and $Ag_2V_4O_{11}$

sample	current density (mA/g)	specific capacity (mAh/g)
nanowires	20	514
	40	461
	80	351
mesowires	20	447
microrods	20	409
bulk particles	20	326
	40	296
	80	234
CuV_2O_6 (ref 11d)	30	329[a]
	30	349[b]
$Ag_2V_4O_{11}$ (ref 23)	31.5	272[c]

[a] The CuV_2O_6 was synthesized by a solid-state reaction. [b] The CuV_2O_6 was synthesized by a solution-based route. [c] The cutoff voltage was 1.5 V.

Figure S9), the electrodes of α-CuV_2O_6 nanowires still retained high capacities of 461 and 351 mAh/g, respectively, which are much higher than that of the electrodes with α-CuV_2O_6 bulk particles. This result reveals that the morphologies and sizes of CuV_2O_6 have a remarkable effect on their discharge capacity and high-rate capability. It is noted that, after storing at 37 °C for 2 months, the discharge capacity of α-CuV_2O_6 nanowires was 510 mAh/g (Supporting Information Figure S10), which is very near to its initial capacity (514 mAh/g), indicating the available long-term stability of the α-CuV_2O_6 nanowires.

Electrochemical Reaction Mechanism. The Cu extrusion mechanism (eq 5) had been proposed to explain the accommodation of lithium in copper vanadate.[9] Since the CuV_2O_6 is composed of Cu^{2+} and V^{5+}, the α-CuV_2O_6 nanowires exhibited some reversibility for the lithium intercalation/deintercalation (Supporting Information Figure S11). However, for the application of primary lithium batteries, the multistep reductions of CuV_2O_6 during lithium intercalation are complex and the accurate reaction mechanisms of CuV_2O_6 with lithium would be more interesting to be understood.

$$CuV_2O_6 + xLi^+ + xe^- \rightarrow Li_xCuV_2O_6 \quad (5)$$

Figure 5a shows the high-resolution XPS spectra of Cu2p and V2p for the fresh-prepared electrode of α-CuV_2O_6 nanowires. Two separate peaks located at the binding energies of 934.7 and 954.5 eV are attributed to Cu^{2+} 2p3/2 and 2p1/2. Meanwhile, a strong satellite peak that appeared at around 942 eV can be ascribed to a typical character of Cu^{2+}. The peaks for

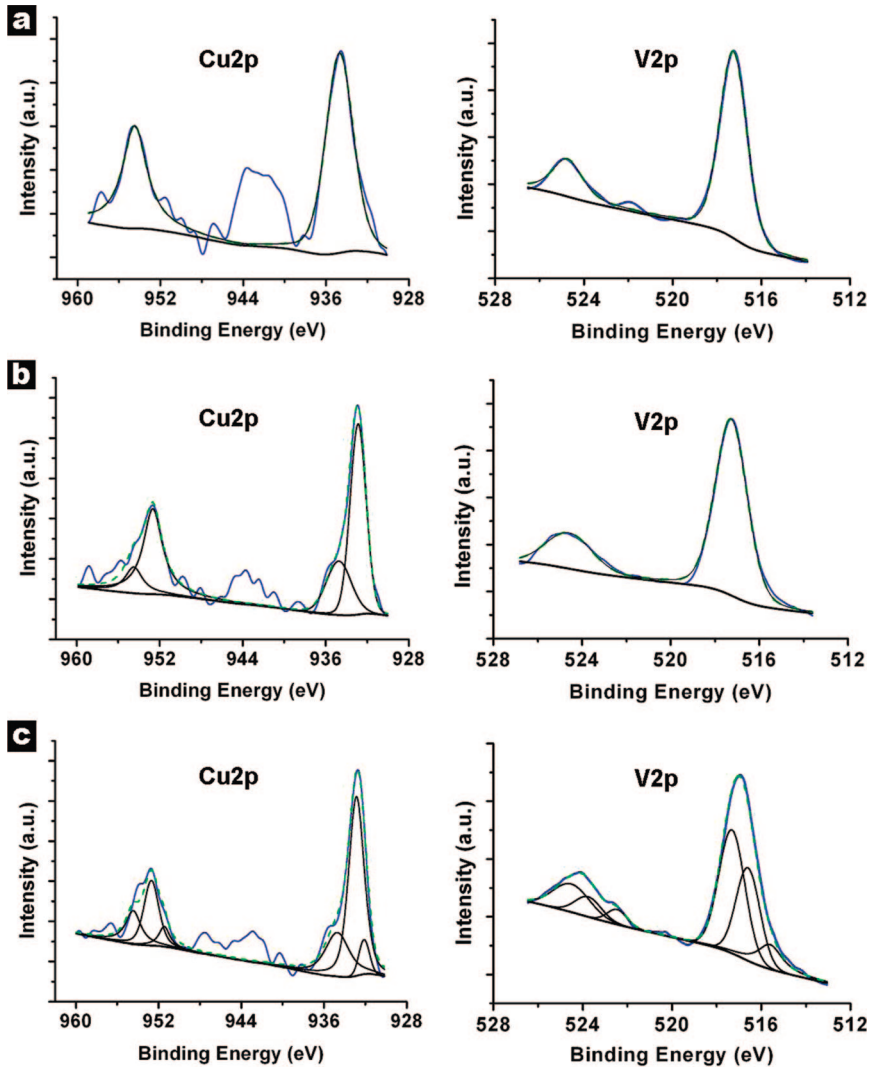

Figure 5. XPS spectra of V2p and Cu2p for the electrode made of α-CuV_2O_6 nanowires at different discharged stages: (a) before discharged, (b) 2.8 V, and (c) 2.3 V. Blue line: raw curve. Green line: fitted data. The survey spectra are shown in Supporting Information Figure S12.

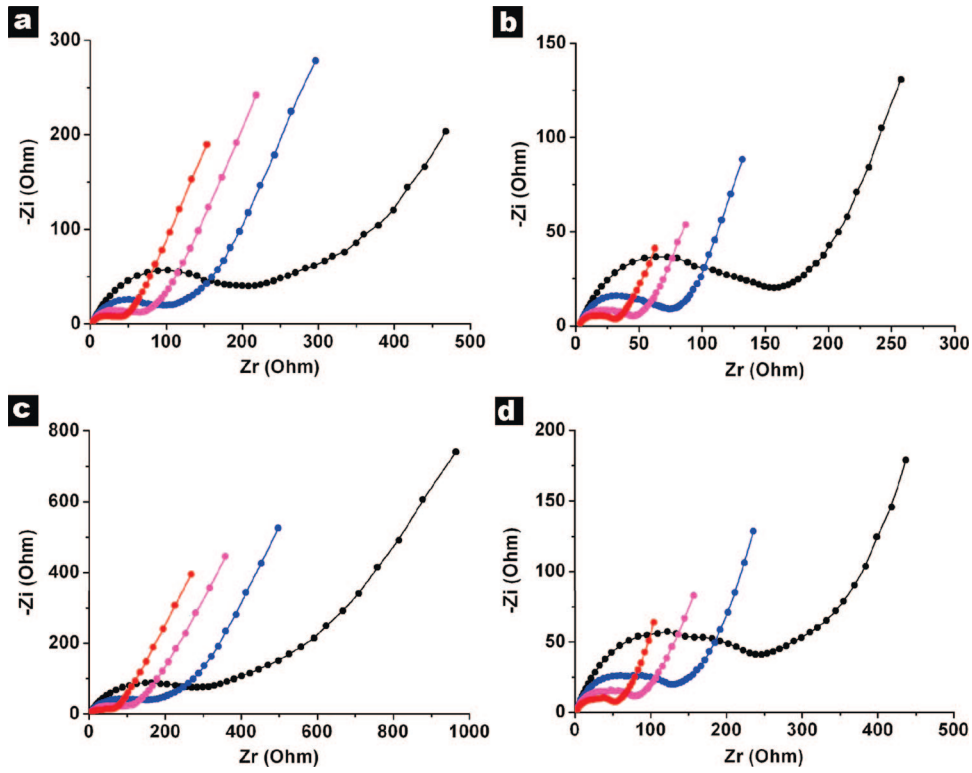

Figure 6. Electrochemical impedance spectra (EIS) for the cells made of α-CuV_2O_6 (a, b) nanowires and (c, d) bulk particles at (a, c) 2.8 V and (b, d) 2.3 V. Temperature = 25 °C (black), 37 °C (blue), 45 °C (magenta), and 55 °C (red).

V2p3/2 (517.3 eV) and V2p1/2 (524.7 eV) can be indexed to V^{5+}. These values of binding energies are consistent with the previously reported results.[23] Therefore, the elements of Cu and V in the as-synthesized CuV_2O_6 nanowires exist as Cu^{2+} and V^{5+}, respectively.

For the electrode discharged to 2.8 V (Figure 5b), the peaks for Cu 2p3/2 and Cu 2p1/2 can be deconvoluted into two components. Besides the existence of Cu^{2+}, two strong doublet peaks of Cu2p appear at the binding energies of 932.9 eV (Cu2p3/2) and 952.7 eV (Cu2p1/2), which are attributed to Cu^+. Moreover, a decrease in the intensity of the satellite peak is observed, revealing that most of the Cu^{2+} is reduced to Cu^+ during the first step of the discharge. In contrast, the XPS spectra of V2p still can be ascribed to V^{5+}.

When the electrode was deeply discharged to 2.3 V (Figure 5c), two new peaks observed at 932.1 and 951.4 eV for Cu2p can be assigned to Cu^0 2p3/2 and 2p1/2, suggesting that the Cu^+ is further reduced to metallic Cu at this discharge stage. Furthermore, the peaks for V2p can be distinguished into three parts. The binding energies of 516.6 and 523.5 eV confirm the formation of V^{4+}. Meanwhile, the characteristic peaks of V^{3+} 2p3/2 and 2p1/2 can be observed at the binding energies of 515.6 and 522.5 eV, indicating that the reduction of V^{5+} to V^{4+} and partial reduction of V^{4+} to V^{3+} occur at the second discharge stage. At the end of the discharge process (2.0 V), the formation of metallic Cu and the morphology of the electrode were further confirmed by XRD and SEM (Supporting Information Figure S13).

On the basis of the above results, an interpretation of lithium intercalation in α-CuV_2O_6 follows. First, the reduction of α-CuV_2O_6 nanowires begins with the reduction of Cu^{2+} in the vanadium-oxide octahedron layers to Cu^+, corresponding to the higher voltage plateau at about 3.0 V in Figure 4. Second, with increasing the discharge depth, the lower voltage plateau at about 2.5 V can be attributed to the dominant reduction of V^{5+} to V^{4+} and further to V^{3+} as well as the partial reduction of Cu^+ to Cu^0, being associated with the extrusion of metallic Cu. Therefore, both the reductions of Cu^{2+} and V^{5+} in α-CuV_2O_6 with lithium intercalation are demonstrated.

Electrochemical Kinetics. To understand the electrode kinetics, the activation energies of the as-prepared α-CuV_2O_6 nanowires for lithium intercalation were estimated by electrochemical impedance spectra (EIS). Figure 6 shows the EIS of the electrodes of α-CuV_2O_6 nanowires and bulk particles at differernt discharge stages and temperatures. In general, the impedance curves present two partially overlapped semicircles in the high- and medium-frequency regions and an inclined line in the low-frequency region. An equivalent circuit used to fit the impedance curve is given in Supporting Information Figure S14, which is similar to the circuit employed for the cathode of the lithium ion battery.[24] The semicircle can be assigned to the combination of the electrode/electrolyte interface film resistance (R_f) and the charge transfer impedance (R_{ct}), while the linear portion is designated to Warburg impedance (W), which is attributed to the diffusion of lithium ions into the bulk of the electrode materials. Then, the exchange currents (i_0) and the apparent activation energies (E_a) for the intercalation of

(22) Beninati, S.; Fantuzzi, M.; Mastragostino, M.; Soavi, F. *J. Power Sources* **2006**, *157*, 483.

(23) (a) Nordlinder, S.; Augustsson, A.; Schmitt, T.; Guo, J. H.; Duda, L. C.; Nordgren, J.; Gustafsson, T.; Edström, K. *Chem. Mater.* **2003**, *15*, 3227. (b) Souza, E. A.; Landers, R.; Tabacniks, M. H.; Cardoso, L. P.; Gorenstein, A. *Electrochim. Acta* **2006**, *51*, 5885.

(24) Yang, S. B.; Song, H. H.; Chen, X. H. *Electrochem. Commun.* **2006**, *8*, 137.

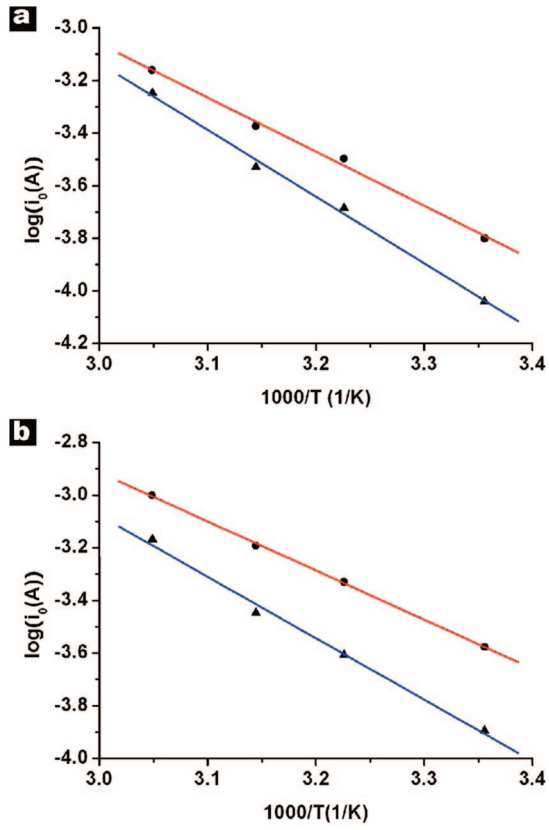

Figure 7. Arrhenius plots of log i_0 versus $1/T$ for the electrodes of α-CuV_2O_6 (circle) nanowires and (triangle) bulk particles at (a) 2.8 V and (b) 2.3 V.

lithium can be calculated by eq 6 and the Arrhenius equation (eq 7), respectively.[1a,25]

$$i_0 = RT/nFR_{ct} \quad (6)$$

$$i_0 = A\exp(-E_a/RT) \quad (7)$$

where A is a temperature-independent coefficient, R is the gas constant, T is the absolute temperature, n is the number of transferred electrons, and F is the Faraday constant. The values of R_{ct} and i_0 for α-CuV_2O_6 nanowires and bulk particles at different temperatures are summarized Table S1. An Arrhenius plot of log i_0 as a function of $1/T$ is shown in Figure 7. On the basis of eq 7, the activation energies ($E_a = -Rk\ln 10$, k = the slope of the straight line in Figure 7) of α-CuV_2O_6 nanowires at 2.8 V (low lithium uptake) and at 2.3 V (high lithium uptake) are calculated to be 39.3 and 35.7 kJ/mol, respectively. In comparison, the activation energies of α-CuV_2O_6 bulk particles at 2.8 and 2.3 V are 48.5 and 44.6 kJ/mol, respectively. The lower activation energies of α-CuV_2O_6 nanowires indicate the shorter diffusion route for lithium intercalation. This enhanced kinetics is due to the fact that the BET surface area of the nanowires (62.1 m^2/g) is much larger than that of the bulk particles (1.6 m^2/g), making the efficient contact of the nanowires with the electrolyte. This surface/interface character decreases the polarization of the electrode and thus increases the discharge capacity and high-rate capability. Moreover, the α-CuV_2O_6 nanowires with an interdigitated porous 3-D network is able to provide an extra space for the diffusion of electrolyte and reduce the stress caused by the cracking of the structure during the discharge process and, thus, suppress the degradation of the electrode.[5,26]

Conclusions

In summary, α-CuV_2O_6 nanowires, mesowires, and microrods have been successfully prepared via a simple hydrothermal approach. The morphologies and sizes of the as-prepared α-CuV_2O_6 were facilely controlled by varying the reaction parameters through a ripening−splitting growth mechanism. The electrochemical results showed that decreasing the diameters of the α-CuV_2O_6 wires is favorable for increasing the discharge capacity and improving the electrode kinetics. The α-CuV_2O_6 nanowires exhibited a high discharge capacity of 514 mAh/g (at the current density of 20 mA/g and the temperature of 37 °C) and a low activation energy of 39.3−35.7 kJ/mol. Furthermore, the XPS and XRD measurements demonstrated the multistep reductions of $Cu^{2+}$and V^{5+} with the intercalation of lithium into α-CuV_2O_6. The present results suggested that nanostructured α-CuV_2O_6 are promising cathode materials in primary lithium battery for long-term and high-rate applications such as in the field of implantable cardioverter defibrillators (ICD).

Acknowledgment. This work was supported by the National Key-Basic Research Program (2005CB623607), NSFC (20703026), and Tianjin High-Tech Development Program (07ZCGHHZ00700).

Supporting Information Available: The illustration of the working principle and configuration of the implantable cardioverter defibrillators (ICD); the picture of the experimental setup; SEM images of α-CuV_2O_6 synthesized from different concentrations of the reactant; SEM images of α-CuV_2O_6 bulk particles obtained from solid-state reaction; XRD patterns and SEM images of α-CuV_2O_6 obtained at different reaction time; illustration of the possible phase transformation in the synthesis of α-CuV_2O_6 nanowires; discharge curves for the electrodes made from the as-prepared α-CuV_2O_6 nanowires and bulk particles at the current densities of 40 and 80 mA/g and the temperature of 37 °C; discharge curves for the electrode made from the as-prepared α-CuV_2O_6 nanowires at the current densities of 20 mA/g after equilibrated at 37 °C for 2 months; cyclic voltammogram (CV) of the electrode made form the α-CuV_2O_6 nanowires in the first cycle at a scan rate of 1.0 mV/s and the temperature of 37 °C; the survey XPS spectra of the electrode made from the α-CuV_2O_6 nanowires at different discharge states; XRD patterns and SEM images of the electrodes with α-CuV_2O_6 nanowires and bulk particles after discharging to the cutoff voltage of 2.0 V; the equivalent circuit for the electrochemical impedance spectrum; table of charge-transfer resistance (R_{ct}) and exchange current (i_0) of α-CuV_2O_6 nanowires and bulk particels measured at different discharge states and temperatures. This material is available free of charge via the Internet at http://pubs.acs.org.

JA800109U

(25) Barsoukov, E.; Macdonald, J. R. *Impedance Spectroscopy Theory, Experiment, and Applications*; John Wiley & Sons: New York, 2005.

(26) Wang, G. L.; Zhang, B.; Wayment, J. R.; Harris, J. M.; White, H. S. *J. Am. Chem. Soc.* **2006**, *128*, 7679.